

Nanoscale Surface Analysis Reveals Origins of Enhanced Interface Passivation in RbF Post Deposition Treated CIGSe Solar Cells

Christian Kameni Boumenou, Himanshu Phirke, Jonathan Rommelfangen, Jean-Nicolas Audinot, Shiro Nishiwaki, Tom Wirtz, Romain Carron, and Alex Redinger*

Alkali post deposition treatments (PDTs) of Cu(In,Ga)Se₂ absorbers have boosted the power conversion efficiency (PCE) of the solar cell devices in the last years. A detailed model explaining how the PDTs impact the optoelectronic properties at the nanoscale is still lacking. Here, via various scanning probe techniques, X-Ray photo-electron spectroscopy and high resolution secondary ion mass spectroscopy it is shown that the RbF PDT treatments lead to a one to one exchange of Rb with Cu at the surface. This exchange takes place in the naturally occurring Cu-depleted CIGSe surface, known as the ordered vacancy compound. A detailed comparison between samples with different PDTs after various cleaning procedures furthermore highlights the necessity to perform all the measurements on NH₄OH cleaning surfaces only. After NH₄OH, no RbInSe₂ phase could be detected at the surface anymore and the surface bandgap, as measured with scanning tunneling spectroscopy is only 1.7 eV. The findings demonstrate that the existence of a RbInSe₂ phase is most likely not responsible for the recent improvements in power conversion efficiency for state of the art solar cells. The primary effect of the PDT treatment is a modification of the ordered vacancy compound, where Cu is exchanged with Rb.

the latest improvements of laboratory scale devices.^[1,3–5] It is therefore of high importance to understand in great detail the interplay of alkali fluorides with the CIGSe surface, grain boundaries and the absorber bulk.

Extensive works over the last years have shown that PDTs always alter the surface composition.^[3,6–8] Especially the Cu-content at the surface is reduced, corroborated by many X-Ray photoelectron spectroscopy (XPS) measurements. In case of multiple alkalis, an ion-exchange mechanism was suggested to take place at the surface^[3] and at the grain boundaries.^[9] Triggered by theoretical calculations, it has been suggested that new alkali-rich compounds are likely to form during the PDT treatment.^[10] These calculations showed that not all alkalis behave the same. The diffusion mechanisms and barriers differ and the tendency to form secondary phases also heavily depends on the alkali-element.

A strong tendency to form AlkInSe₂ compounds was identified for Alk=K, Rb, Cs, whereas the lighter elements, such as Na, Li are more likely to only substitute Cu in the CIGSe structure. Especially the existence of a RbInSe₂ was identified at the surface of the absorbers via transmission electron microscopy measurements.^[11] The measurements also showed that the existence of this phase depends on the Cu-content. XPS measurements revealed a K-In-Se rich surface^[6,12] or a Rb-In-Se surface after KF/RbF PDTs.^[13] These AlkInSe₂ phases are considered to play an important role for surface passivation.

1. Introduction

Cu(In,Ga)Se₂ (CIGSe) thin film solar cells have achieved excellent power conversion efficiencies (PCE) in the laboratory and on the module level. The current record PCEs are 23.4% on small areas,^[1] 19.6% on 30×30 cm² mini-modules^[2] and 19.2% for modules, which highlights the potential of this technology. Alkali fluoride post deposition treatments (PDTs) of KF, RbF, and/or CsF have played a crucial role in all of

C. K. Boumenou, H. Phirke, J. Rommelfangen, A. Redinger
Department of Physics and Materials Science
University of Luxembourg
Luxembourg L-1511, Luxembourg
E-mail: alex.redinger@uni.lu

J.-N. Audinot, T. Wirtz
Advanced Instrumentation for Nano-Analytics (AINA)
Luxembourg Institute of Science and Technology
41 rue du Brill, Belvaux L-4422, Luxembourg

S. Nishiwaki, R. Carron
Laboratory for Thin Films and Photovoltaics Empa-Swiss Federal
Laboratories for Materials Science and Technology Ueberlandstrasse 129
Duebendorf CH-8600, Switzerland

 The ORCID identification number(s) for the author(s) of this article can be found under <https://doi.org/10.1002/adfm.202300590>.

© 2023 The Authors. Advanced Functional Materials published by Wiley-VCH GmbH. This is an open access article under the terms of the Creative Commons Attribution License, which permits use, distribution and reproduction in any medium, provided the original work is properly cited.

DOI: 10.1002/adfm.202300590

Density function theory calculations also showed that Na and K can be incorporated in the CuIn_5Se_8 matrices where they occupy Cu vacancies.^[14] The negative formation energies suggest that this process will form spontaneously at low impurity concentrations. In addition, the formation of K-K or Na-Na dumbbells and interstitials are also energetically favorable. For the case of Rb, it has recently been shown that Rb atoms can occupy the near surface region of the CIGSe absorbers where they substitute Cu.^[15] Importantly, the calculations showed that the incorporation of Rb reduced the incorporation of oxygen, thereby improving the passivation.

However, some of the results are still debated. The formation of the AlkInSe_2 phase depends on the Cu-content and to a certain extent also on the details of the synthesis routine.^[16,17] Some reports clearly identify a modification of the conduction and valence band position due to PDT whereas others did not observe this effect.^[17,18] The impact of the alkalis on grain boundaries are not clear either. Several high resolution techniques revealed a preferential segregation of the alkalis at the grain boundaries.^[19–21] Some reports show a reduction in grain boundary band bending.^[9] Nevertheless, the recombination velocities are still high at the grain boundaries, which points toward an ineffective passivation.^[22] The concentration of alkalis in the bulk is low. Nevertheless a strong impact of the PDT treatment on quasi-Fermi-level splitting has been reported. The correlation of Urbach energy^[23] and band bending^[9] hints toward a modification of the grain boundary properties.^[17] However, some of the KPFM measurements have been performed in amplitude modulation mode, which is prone to show artifacts at grain boundaries on rough surfaces.^[24]

The modification of the absorber surface due to the PDTs also affects the subsequent layers of the solar cell. The deposition of the CdS buffer layer is modified in such a way that a thinner layer can be used in the highest performing solar cells.^[3] This reduces the parasitic light absorption in the buffer layer and the short circuit current density is increased. The V_{OC} and quasi Fermi-level splittings^[5,25] also increased, which points toward a better defect passivation^[26] and/or higher doping.^[27–29]

The most problematic point however is one that is rarely discussed in literature. The measurements are almost never done under the same conditions. Some results were acquired on absorbers rinsed with H_2O , whereas for others an NH_4OH rinsing was applied. Some authors cleaned the samples with diluted HCl or KCN solutions. Even others did not specify the cleaning at all. In Supporting Information, we summarized in a table 56 different studies where we checked how the sample was prepared prior to the XPS measurements. The table underlines the lack of consistency throughout the literature. This is problematic since the different surface treatments are likely to play a crucial role during the subsequent formation of the p-n-junction. The development of new buffers and passivation strategies critically depend on the surface state prior to the growth process. Consequently, it is important to understand, which treatment does what and how this leads to a clean and well defined CIGSe surface.

Furthermore, the comparison of results from different laboratories, after different cleaning steps is likely to lead to an erroneous interpretation. It is therefore vital to compare measurements carried out after different surface treatments in

order to link the results to the available literature. On top of that compositional variations need to be correlated with electrical and optical properties after each treatment. In addition, it is absolutely vital to combine methods with a high chemical sensitivity and techniques with high lateral resolution. These results then need to be linked to measurements of the optoelectronic properties of the absorber in order to gain a full picture of the changes induced via PDTs.

In this article we aim to exactly carry out such an exercise where we use two techniques with a high chemical sensitivity, that is, X-Ray photo-electron spectroscopy to quantify the composition at the surface and secondary ion mass spectroscopy mapping performed on a Helium ion microscope (HIM-SIMS) to identify chemical inhomogeneities with nanometer spatial resolution.^[30] These results will be compared to atomic force microscopy (topography) and Kelvin probe force microscopy (KPFM). The chemical changes can thereby be correlated with laterally resolved workfunction maps. The surface bandgap and the density of states of the valence and conduction bands are assessed with scanning tunneling spectroscopy (STS). Complementary measurements are done via Raman spectroscopy to identify fingerprints of secondary phases at the surface of the absorber. This unique combination of techniques will be applied to absorbers after various stages ranging from as-grown to H_2O and NH_4OH -rinsed samples. In order to understand the impact of our results on device performance we use SCAPS simulations.^[31]

We will discuss how the surface composition changes after the different cleaning steps, when we observe secondary phases at the CIGSe surface and how those can be removed. The STS measurements allow us to correlate the different surface compositions to a surface bandgap. Finally, we will develop a consistent model, which combines the results from our various surface sensitive techniques.

2. Results

2.1. Chemical Composition of the Near Surface Region

The different samples and all the characterization techniques used in this study are summarized in the Experimental Section. The XPS survey spectra of the RbF PDT treated samples after the various surface treatments are depicted in **Figure 1** whereas the spectra for the NaF treated films are summarized in Figure S1 (Supporting Information). The spectra were normalized to one and vertically shifted to enhance the visibility. The XPS core levels of the various elements are highlighted with vertical orange lines, whereas the Auger lines are depicted in blue. The spectrum of the as-grown surface was dominated by sodium and fluorine related compounds. In addition, small amounts of Se, In, and Rb could be identified on the surface of the absorbers. Oxygen and carbon were also identified at the surface, which were attributed to surface contamination. The NaF treated films showed similar surface compositions, with the exception of a lack of Rb.

After H_2O rinsing, Na and F related signals completely disappeared (see Figure S4, Supporting Information). However, the sample surface did still not exhibit a bulk CIGSe composition,

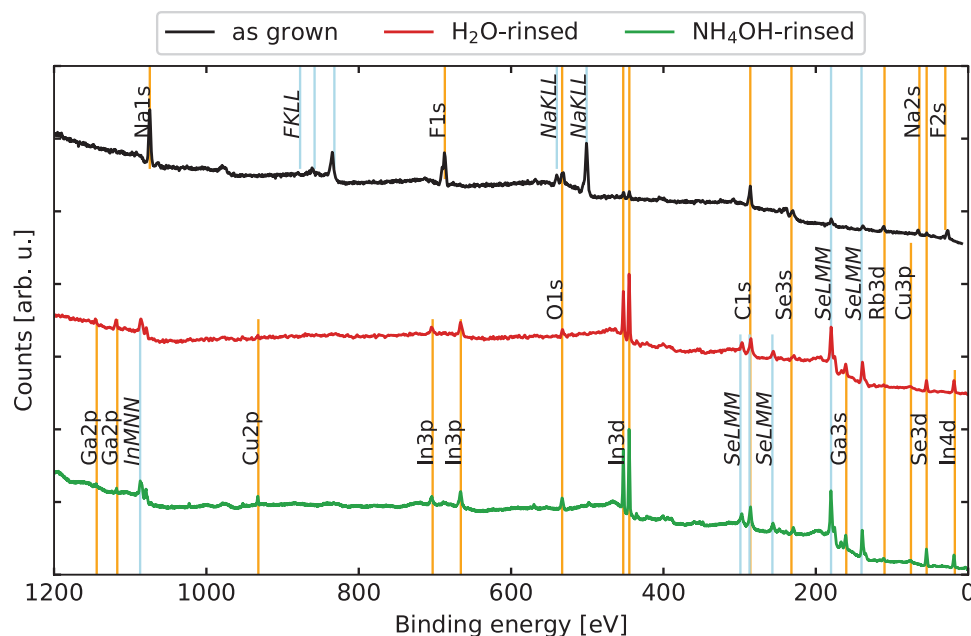


Figure 1. Survey spectra of RbF PDT treated CIGSe films measured without cleaning, after water and ammonia rinsing. All spectra were normalized for better visualization. The orange lines highlight the position of the XPS core levels, whereas the blue ones are Auger transitions for the various elements.

since the Copper and Ga signals were very low. A small amount of Rb was also detected after H_2O rinsing suggesting a distinct binding mechanism of Rb compared to Na, which was removed completely. These results were mostly in agreement with previous reports who showed a strong Cu and Ga depletion after the heavy alkali PDT treatments.^[13,32–34] In the CIGSe community, these observations have triggered numerous studies focused on Cu depleted surfaces after PDT treatments. Modeling of depth dependent XPS measurements suggest a very thin RbInSe_2 phase on top of a Cu-depleted CuIn_5Se_8 phase.^[13] The resulting thickness of the RbInSe_2 thereby depending sensitively on the amount of Rb deposited during the PDT treatment. For the standard deposition times best fits of the RbInSe_2 thickness amounted to only 0.1 nm, that is, lower than a single monolayer (0.8 nm).^[13]

In literature, there is not general consensus on whether a wet cleaning is indispensable for high efficiency CIGSe. Some reports show that an additional NH_4OH / H_2O cleaning is mandatory^[35,36] whereas others could produce high efficiency solar cells without any additional treatment.^[37] The necessity to clean the surface from Na and F precipitations seem to be linked to the type of buffer layer that is used to make the devices. For the case of wet buffer layers (CdS or $\text{Zn}(\text{S},\text{O})$) the CIGSe surface is always washed with H_2O and NH_4OH . Independent of the reported power conversion efficiencies, reports have shown that the near surface region undergoes an additional change in composition during cleaning.^[35]

The survey spectrum in Figure 1 underlines this result. Especially, a clearer Cu signal is visible after the NH_4OH treatment, which highlights another compositional change of the near surface region upon surface cleaning. However, the survey spectrum does not allow for a detailed analysis of the peak shapes. Therefore, high resolution measurements of the regions

of interest were carried out and presented in Figure 2 and Figures S2 and S3 (Supporting Information).

The high resolution XPS spectra of $\text{Rb}3\text{d}$, $\text{In}3\text{d}$, and $\text{Se}3\text{d}$ are discussed in the following since they exhibit various interesting features after each treatment. The deduced binding energies are tabulated in Supporting Information. The spectra were analysed as follows. In a first step each spectrum was inspected and the number of peaks was determined. Here, it has to be emphasized that we only took into account obvious shoulders and peak distortions. Especially for the H_2O and NH_4OH rinsed samples, it was not obvious at first sight if the measured peak arose from a single chemical environment or multiple ones. This can be seen well for the case of Se in Figure 2f,i. The spectrum in Figure 2f could either be fitted with a single oxidation state or two different oxidation states. The only change would have been the used FWHM of the doublet.

However, the FWHM of the Se core level after NH_4OH washing was slightly smaller than after H_2O washing. Since the width of the peaks in XPS depends on the experimental constraints (XPS detector resolution, electronic lenses, aperture etc.) the smallest FWHM characterises the film with the least number of secondary phases. For the case of the $\text{Se}3\text{d}$ core level, the spectrum after NH_4OH treatment can be fitted with one chemical environment only. Later in the manuscript, when we discuss the AFM and KPFM results we will see that this approach is well justified. As soon as the lowest FWHM for each element was identified all the peaks were analyzed with this constrain. In case where the fitting did not result in a satisfactory result, an additional peak was included as shown for the case of the $\text{Se}3\text{d}$ peak after H_2O rinsing. In addition to the constant FWHM for each element the peak shape and the background shape was also kept constant. The results of this analysis is summarized in Figure 2.

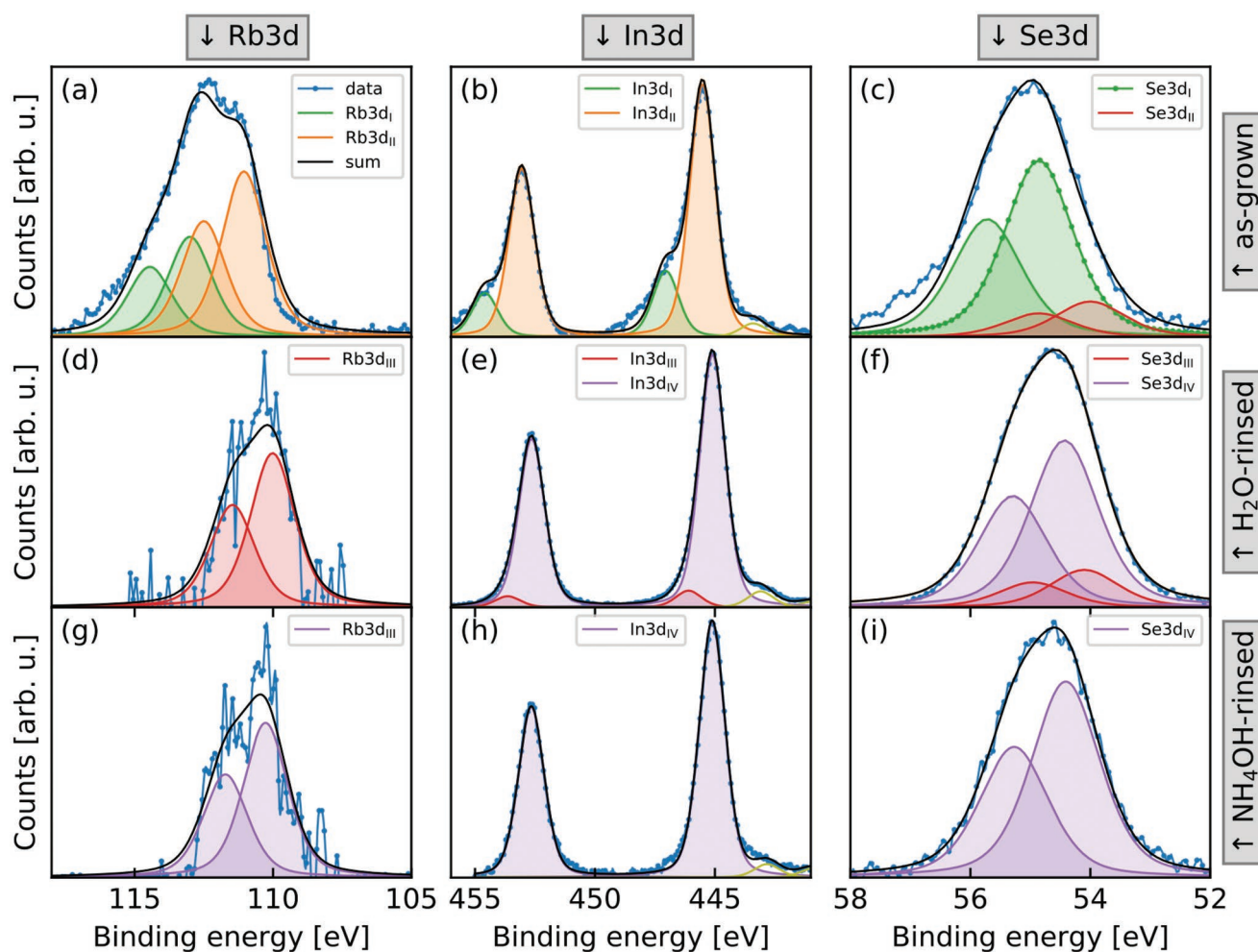


Figure 2. High resolution XPS spectra of Rb3d, In3d, and Se3d after the RbF PDT, after H₂O and NH₄OH cleaning. The yellow peak visible in the In3d spectrum (below 445 eV) is a satellite peak arising from the X-ray source and is not considered for the quantification.

For convenience purposes, each distinct chemical environment was labeled with a roman number and the values given in the following will always refer to the highest peak of the spin doublet, that is, the 5/2 spin state for the Se, In, and Rb d core levels. For the as-grown sample two different Rb chemical environments could be identified with binding energies (BE) at 113.0 eV (Rb3d_I) and 111.1 eV (Rb3d_{II}). After H₂O-washing the spectrum reduced to a single doublet with a BE=110.0 eV (Rb3d_{III}). The Rb3d_I and Rb3d_{II} signals disappeared. The nature of the compounds I and II can therefore be linked to residues that were not incorporated in the CIGSe matrix and which can be dissolved in H₂O. Possible candidates are RbSe and/or RbF. NH₄OH washing did not fully remove the Rb from the surface and a fit to the Rb3d doublet results in a binding energy of 110.3 eV. Due to the low signal to noise we leave the labeling identical to the case after H₂O washing, that is, (Rb3d_{III}). It is probable that the signal after H₂O washing consists of two doublets. However, we are unable to resolve this detail in the spectra. The deduced Rb binding energies after H₂O and NH₄OH are well within the range of the reported ones^[32] where two different Rb species with binding energies of 110.5 and 110.0 eV were reported. Although we did not attempt to fit the

spectra with two different species, we note that the trend is in accordance with literature where the 110.5 eV was less stable against NH₄OH cleaning. In our case, we did observe a shift from 110.0 to 110.3 eV.

The indium data exhibited a similar diversity in peaks. The as-grown samples showed two different In compounds at a BE=447.1 eV and BE=445.5 eV denoted as In3d_I and In3d_{II}. After washing the samples with H₂O, again two doublets were identified labeled as In3d_{III} and In3d_{IV}, albeit shifted to lower binding energies. After washing with NH₄OH, the In3d_{III} was absent and only In3d_{IV} was left. The fitting was done by keeping the position of the In3d_{IV} at the fixed binding energy position for the H₂O and NH₄OH. The reasoning here is that for both surfaces, H₂O and NH₄OH, the majority of the surface consists of a Cu-depleted CIGSe. Consequently, the In3d_{IV} must be situated at the same binding energy. This assumption is strengthened by analysis of the Auger parameter, which is not influenced by surface charging or band bending. The Auger parameter, which is defined as $\alpha' = E_k(C_1C_2C_3) + E_b(C)$ is often used for chemical state analysis in XPS.^[38] The kinetic energy is denoted as E_k , the binding energy as E_b , C refers to the involved core level and C_i , $i=1..3$ to the involved core levels of the Auger

transition. The calculated value of α' after NH_4OH cleaning for In 4d_{5/2}, $\text{M}_4\text{N}_{45}\text{N}_{45}$ equals to 425.3 eV, in excellent agreement with^[13] who identified this as the Auger parameter of CIGSe. As a side-note, we like to mention that the ghost peak in the In3d spectra with a binding energy of 442.8 eV was due to the non-monochromatic Al K α X-Ray source.

Finally, the Selenium 3d core level of the as grown films was modeled by two chemical states at BE=54.0 eV (Se3d_I) and BE=54.9 eV (Se3d_{II}). After H_2O washing Se3d_I and Se3d_{II} disappeared and were substituted with Se3d_{III} and Se3d_{IV} . Again, a shift toward lower binding energies was observed. After NH_4OH washing, Se3d_{III} was absent and only Se3d_{IV} was left. α' for $\text{Se3d}_{L3}\text{M}_{45}\text{M}_{45}$ equals to 1361.2 eV, which is again in excellent agreement with a CIGSe surface.^[13] The binding energy of Se3d core level after NH_4OH cleaning was in good agreement with literature.^[39] In that report a very systematic study of the Se core levels after different chemical treatments was discussed. The authors reported that, after NH_4OH cleaning, the CIGSe surface was composed of at least two different Se species, related to bulk CIGSe and the Cu-depleted layer. In the present case this could not be verified since the resolution of the used XPS system in this study was inferior to the one used in ref. [39].

CIGSe absorbers subjected to a RbF PDT showed an additional Selenium species at lower binding energies compared to the CIGSe one.^[32] This observation is in line with our results where we also identified a second Se species (Se3d_{III}) after H_2O cleaning, which could not be identified anymore after NH_4OH cleaning. This is in contrast to ref. [32] where the second Se core level with low binding energy was still present after NH_4OH cleaning. The difference might be due to a slightly different Cu-content of the CIGSe absorber and to a certain extend also on the ultimate resolution and signal to noise ratio of the XPS system.

The surface compositions, as calculated from the XPS spectra are presented in Table 1. For the quantification, we used the Cu2p, In4d, Ga3d, Se3d, and Rb3d core levels. In Table 1 the second row indicates the core level that was used for the quantification. If nothing is in a column then the values from the preceding columns were used. The photoionization cross sections for each element were taken from ref. [40]. For all samples we find, very Cu-poor surfaces, in agreement with literature (see column 7). For all ratios (except the last column) we used the sum of all measured counts from each element for

the quantification. The quantification with the In3d compared to the In4d gives only slightly different values mainly due to the difference in the inelastic mean free path. We therefore chose the In4d peak here, since then the Ga and In signal originate from the same binding energy region.

We have not carried out the quantification for the as-grown sample since here the measured surface composition does not correspond to CIGSe (mostly Na, F, and Se was detected) and therefore the computed ratios are only of minor interest.

Comparing the Cu/(In+Ga) ratios on the two sets of samples we observe that the Cu signal is lower on the RbF-PDT sample compared to the NaF sample (see column 7). This observation is also in line with literature. We measured a much larger amount of In on the surface of the RbF-PDT sample compared to the NaF-PDT one, which reduced substantially after the NH_4OH treatment. Furthermore, the Ga-signals are larger for the NaF sample compared to the RbF sample. This becomes obvious when comparing column 7 and 8 of Table 1. The Cu/(In+Ga) ratios are different than the Cu/In ratios for the case of the NaF treated samples but almost identical for the case of the RbF treated sample.

It is known that on the NaF sample an ordered vacancy compound (ODC) like phase exists at the surface, with Cu/In ratios of 0.33 for a CuIn_3Se_5 compound or 0.2 with for a CuIn_5Se_8 compound. Our experimental results are in good agreement with this assumption, since we find a value of 0.2, which is compatible with a CuIn_5Se_8 phase. We would like to note here that we do not infer from these results that the phase is indeed a CuIn_5Se_8 phase. Within the errorbar of the XPS measurements both compositions, or even a mixture of both would explain the measured values.

For the RbF-treated sample this is not the case and we find Cu/In ratios in the order of 0.05 (column 8), which is not compatible with an ODC composition. Most reports in literature therefore assume that a RbInSe_2 phase exists at the surface, with a Rb/In=1. The measured surface composition in our case is however far off as we find a value of 0.1 for the H_2O rinsed sample and 0.2 for the NH_4OH cleaned sample (see Rb/In ratios in Table 1(column 11)). Another option to explain the experimental data is that the Cu included in the ODC phase is replaced by Rb. The (Cu+Rb)/In should then be close to the ODC ratio measured on a RbF-free sample. The calculated composition is in excellent agreement with this assumption, as highlighted in blue in Table 1 (compare column 8 with

Table 1. Surface composition, as determined from the XPS measurements performed on H_2O and NH_4OH treated samples. The indicated XPS core level lines indicated in the table (line 2) were used for the quantification. The blue values highlight that the Cu/(In+Ga) ratio on the NaF samples are very close to the (Cu+Rb)/In ratios on the RbF-treated samples after NH_4OH rinsing. The calculated ratios were computed from the Cu2p, In4d, Ga3d, Se3d, and Rb3d core levels. The only exception was the use of the In3d_{III} component to calculate the stoichiometry of the In related secondary phase after H_2O cleaning.

	Cu [at%]	In [at%]	Ga [at%]	Se [at%]	Rb	$\frac{\text{Cu}}{(\text{In} + \text{Ga})}$	$\frac{\text{Cu}}{\text{In}}$	$\frac{\text{Cu} + \text{Rb}}{\text{In} + \text{Ga}}$	$\frac{\text{Cu} + \text{Rb}}{\text{In}}$	$\frac{\text{Rb}}{\text{In}}$	$\frac{\text{Rb}}{\text{In}_{3d_{III}}}$
XPS line	2p	4d	3d	3d	3d					4d	3d _{III}
NaF (H_2O)	6	33	13	48	–	0.1	0.2	–	–	–	–
NaF (NH_4OH)	7	34	7	52	–	0.2	0.2	–	–	–	–
RbF (H_2O)	2	46	1	48	4	0.04	0.04	0.1	0.1	0.1	1.6
RbF (NH_4OH)	2	37	4	52	6	0.05	0.05	0.2	0.2	0.2	–

column 10). Consequently, our XPS results suggest a modified ODC phase and not a RbInSe_2 phase on the surface after PDT and NH_4OH etching.

The final question to answer from this set of XPS measurements is, if the second phase we measured on the H_2O cleaned sample would be compatible with a RbInSe_2 phase. Therefore, we computed the atomic ratios of Rb/In for the $\text{In}_{3d_{III}}$ signal only, that is, the indium included in the secondary phase. As shown in Figure 2e, this peak was only visible on the H_2O treated sample and vanished after NH_4OH treatment.

The value is 1.6 (column 12; $\text{Rb}/\text{In}_{3d_{III}}$), which is reasonably close to the expected value of 1 given the large uncertainties of the computed ratios. Consequently our XPS results are in principle compatible with a thin RbInSe_2 phase after H_2O cleaning, which was removed after the NH_4OH treatment. The existence of this phase however needs to be corroborated with other high resolution techniques, as discussed below in order to make a definite statement.

Until now, we have only looked at the integral surface composition with XPS. A microscopic view is missing. In literature a partial coverage of a RbInSe_2 after H_2O washing was proposed.^[13] If this is correct, then we should be able to identify

traces of such a phase with the help of AFM/STM and HIM/SIMS. Furthermore we need to corroborate that the RbF sample after H_2O cleaning exhibited a RbInSe_2 phase, which was removed/strongly reduced compared to the NH_4OH , as suggested by the two observed doublets in the In_{3d} and Se_{3d} core levels. Therefore, we will proceed with an AFM analysis to study the occurrence of secondary phases, nanometer resolved SIMS mapping to study spatial correlations in the elemental compositions and STM and STS measurements to link the surface composition to a surface bandgap.

2.2. Analysis on the Nanometer Scale

The AFM and KPFM analysis carried out on the Rb -treated absorbers is presented in Figure 3. All the measurements were carried out in a nitrogen environment to avoid heavy oxidation and the tip work function was calibrated with an HOPG reference sample. Complementary measurements performed on NaF PDT-treated samples are shown in Figure S5 (Supporting Information). The topography data (Figure 3a–c) showed different morphologies as a function of the surface treatment. The

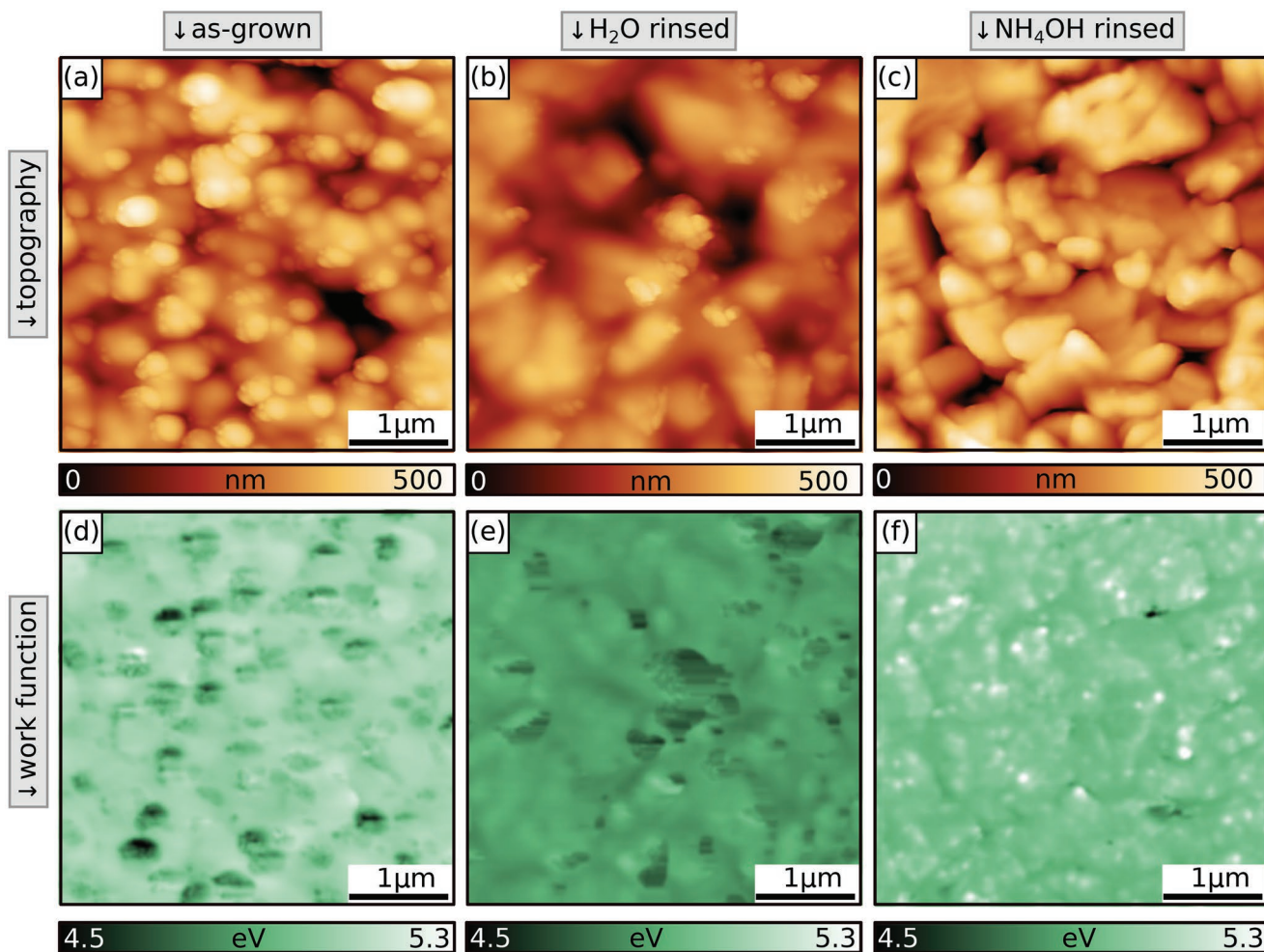


Figure 3. AFM surface topography images and simultaneously measured KPFM work function maps of the RbF PDT treated CIGSe. a, d) are as-grown samples. b, e) are H_2O rinsed samples. c, f) are NH_4OH rinsed samples.

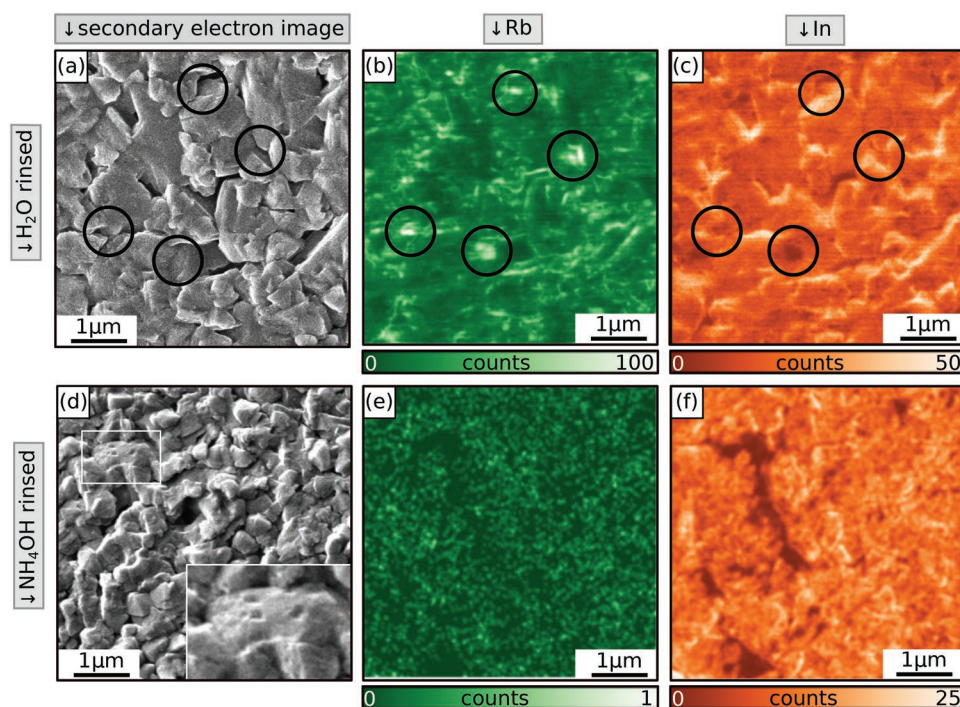


Figure 4. a,d) secondary electron images, b,e) SIMS maps of Rb, and c,f) SIMS maps of In after water rinsing (top row) and NH₄OH rinsing (bottom row)

as-grown samples exhibited a large number of small circular shaped grains, which were absent after NH₄OH cleaning. This already points toward a secondary phase present at the surface of the as-grown and probably also of the H₂O cleaned films.

However, the AFM data alone does not allow to identify possible secondary phases. Therefore, KPFM measurements were carried out and the results for exactly the same regions shown in Figure 3a–c are presented in Figure 3d–f. In the KPFM measurements we could clearly identify regions with different work functions. The granular structures, covering approximately 45% of the as-grown surface exhibited a lower work function (<4.8 eV) as compared to the average work function (5.0 eV) of surface.

After H₂O rinsing, we observed a reduction in the density of the low work function structures, indicating a removal of these surface residues. However, the measurements clearly showed that rinsing the alkali post-treated CIGSe with only distilled water was not sufficient to remove this secondary phase completely. The coverage of the structures was reduced to about 27% with a low work function value of 4.6 eV. The work function of the remaining surface also changed and reduced from 5.0 eV to 4.8 eV. In contrast to the RbF PDT treated samples the NaF-PDT samples showed a complete removal of all the residues after H₂O rinsing (see Figure S5, Supporting Information) suggesting that the remaining residues observed on the RbF treated samples after H₂O rinsing were due to the formation of Rb-related compounds on the surface.

After cleaning the surface with NH₄OH, the secondary phase was removed completely and in the KPFM data we could not detect low work function regions anymore. The topography finally showed well defined grains and the small precipitates were absent. Interestingly, the average workfunction increased

from 4.8 to 5.0 eV suggesting another surface modification. In addition, we could identify regions with a slightly higher work function of 5.3 eV. These regions were completely absent on the H₂O treated surfaces. In contrast to other reports,^[41] we did not see the formation of voids in AFM after NH₄OH washing. Such voids were often observed in scanning electron microscopy measurements (SEM) of CIGSe surface after surface cleaning. The change in workfunction between the H₂O and NH₄OH treated absorber suggests that there was a surface modification taking place, which will be discussed later in this manuscript. The origin of the small white dots (work function ~ 5.3 eV) are at present not clear.

From the AFM and KPFM measurements, we can corroborate that the surface is indeed modified substantially after each cleaning step in accordance with the XPS analysis discussed before. In XPS, we were able to identify two different compounds at the surface of the H₂O rinsed surface, which were labeled In₃d_{III} and Se₃d_{III}, respectively. This secondary phase was tentatively assigned to a RbInSe₂ phase based on the available literature and the measured atomic concentrations. The AFM/KPFM measurements suggest that this secondary phase was removed after NH₄OH washing (disappearance of the low work function areas). This disappearance of the low work function areas agrees with the XPS measurements where the In₃d_{III} and the Se₃d_{III} were not visible after NH₄OH treatment anymore.

This would imply a reduction of Rb/In rich domains at the surface after NH₄OH rinsing. In order to corroborate this assumption, we carried out SIMS measurements to measure with high sensitivity the changes in the Rb and In at the surface.

The helium ion microscopy images and the corresponding SIMS maps of the RbF-treated absorbers after H₂O and NH₄OH cleaning are depicted in Figure 4. The samples were

shipped to the instrument in N_2 and measured in high vacuum to minimize oxidation. The data of NaF PDT treated CIGSe absorbers can be found in Figures S6 and S7 (Supporting Information). In Figure 4, the results for the Rb and In signal are shown. The Ga and Na signals were also collected and can be found in Figures S8 and S9 (Supporting Information). The elemental map of the Cu was omitted here since the concentration and the ionization probability of Cu at the surface were low and no reliable signal could be detected. Comparing the measured Rb and In counts after the different cleaning steps showed that there was a larger amount of Rb present on the CIGSe surface after H_2O washing, which was reduced after NH_4OH cleaning. The Indium signal on the other hand did not change much. It is not possible to deduce concentrations from the SIMS data directly, without elaborate calibration steps. Therefore, we cannot quantify the changes of the Rb content at the surface but we will only discuss the results qualitatively. The lack of quantification is related to the extreme sensitivity of the ionization probabilities to oxygen and small changes in composition of the matrix elements.

The SIMS measurements did not reveal a strong correlation between Rb and In, which would have been expected in case of a $RbInSe_2$ layer. The computed Pearson correlation coefficients,^[42] which allow to measure the linear correlation between two quantities was only 0.07 for the H_2O rinsed sample and 0.1 for the NH_4OH rinsed absorber, which is low considering that a coefficient of 1 indicates a perfect correlation. On the other hand the Ga and In correlation was strong (0.86) for water rinsed sample and still high but slightly reduced (0.49) after ammonia etching, which makes sense considering that the dominating matrix was CIGSe.

However, we did observe some agglomerations, which exhibited a higher concentration of Rb (circles in Figure 4b). These regions also showed a reduced value of In and Ga. Again, we cannot estimate the concentration from the intensity changes in SIMS, however, we can conclude that some regions of the H_2O rinsed samples exhibited patches with an increased amount of Rb. The size of these patches was similar to the observed ones in AFM after H_2O rinsing (Figure 3b,e). In accordance with the AFM data, the patches disappeared after the NH_4OH cleaning step.

The SIMS results, thereby confirmed that the near surface composition was altered after H_2O washing but a clear $RbInSe_2$ phase could not be detected. This might be due to the different ionization probabilities of the probed elements, coupled with the very low thickness of the secondary phase. A monolayer thick $RbInSe_2$ phase on top of CIGSe would not be easy to disentangle if we assume that the SIMS signal is an average of the first 2–3 nm of the film. However, the combination of KPFM and SIMS indicates that the residues after H_2O are indeed Rb-rich, in agreement with the XPS analysis.

On the H_2O cleaned sample we do see a rather strong grain boundary contrast in the Rb signal, suggesting preferential accumulation at the grain boundaries (Figure 4b). However, we observed similar enhancements at the edges of the grains for In and Ga (Figure 4c; Figure S8d, Supporting Information). At first sight, this points toward a SIMS artefact, where the secondary ion yields are enhanced at the grain boundaries due to an increase of the sputter yields at these locations. However,

the topography induced contrast is drastically reduced for the NH_4OH cleaned surface, where more uniform Rb, In, Ga yields were measured. We interpret this as follows. The excess Rb present at the surface after H_2O cleaning acts as a trap for oxygen. It is well known that secondary electron yields in SIMS increase in the presence of oxygen. Consequently, the higher amount of Rb at the surface after H_2O cleaning compared to the NH_4OH yields higher In and Ga signals. Since more Rb is present at the grain boundaries, the signals of all elements measured in positive mode are also enhanced due to a preferential chemisorption of oxygen at these locations. The NH_4OH rinsing removed some of the Rb at the surface and at the grain boundaries, which thereby reduces the topography induced cross-talk in the Ga and In signals too.

After NH_4OH we found a more uniform distribution of Rb. However, some regions did show slightly reduced In, Ga and Rb signals. For one of these regions, we could also observe some small “holes” in the secondary electron image (inset Figure 4d), similar to ref. [41]. This points toward an incomplete or facet dependent distribution of Rb. It makes sense that the slight reduction in Rb also reduces the In and Ga signals, as previously discussed. However, we stress that most of the surface is uniform and the “hole” like structures are not dominating the NH_4OH cleaned surface.

We have also observed some fluorine patches in our SIMS mapping (see Supporting Information) both on H_2O and NH_4OH cleaned surfaces. Correlation maps with Rb and F were not possible as these elements were measured in different acquisition modes. The fluorine concentration is below the detection limit of the XPS, since we have not observed any trace after H_2O and NH_4OH cleaned surfaces. F has a very high probability to ionise into F^- during the emission process, leading to very low detection limits for F in SIMS. This means that even the tiniest F contamination will trigger a F^- signal in SIMS. At present, we cannot conclude on the impact of these minor F precipitates on device performance.

Until now, we have developed a detailed picture of the compositional changes at the surface of the CIGSe absorbers after the different chemical treatments. The analysis of the electronic properties is still missing. One of the only techniques, that allow at the same time mono-layer sensitively, nanometer scale resolution and direct access to the density of states at the valence and conduction bands is STM and STS. The same set of samples has therefore been measured with this technique and the results are discussed next.

Figure 5 depicts STM topography images of the RbF treated CIGSe layer after water (Figure 5a) and after ammonia (Figure 5e) cleaning. The corresponding local density of states (dI/dU -CITS) maps at different specific applied voltages are displayed in Figure 5b–d for the water rinsed and in Figure 5f–h for ammonia washed sample. The STM measurements for the NaF-PDT sample are shown in Figure S10 (Supporting Information).

The scale bar below each sub-figure indicates either the height or the magnitude of the dI/dU changes across the surface. The scale was optimized for the best possible contrast. We chose to display the dI/dU -CITS maps at $U=-1$ V, 0 V, and 1 V for the following reasons. First, we would like to explore the distribution of the LDOS at the Fermi-level, that is, at $U=0$ V.

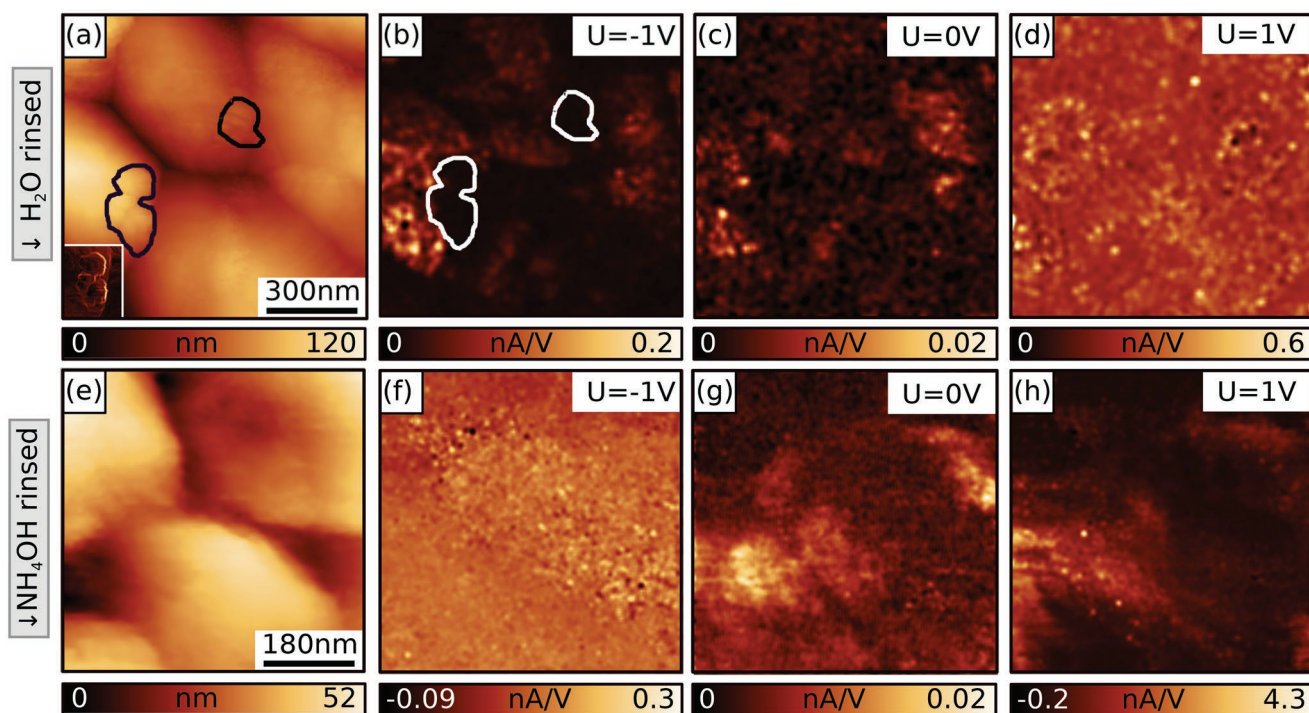


Figure 5. a) STM topography image of the H₂O cleaned sample; b–e) dI/dU -CITS of the same spot at -1, 0, and 1 V; (e) STM topography image of the NH₄OH washed sample; f–h) corresponding dI/dU -CITS at -1, 0, and 1 V. The scale bar below each sub-figure was optimized to have the best possible contrast for each analysis area.

Second, the dI/dU -CITS maps at positive and negative voltages allows to visualize changes close to the conduction and valence band.

Similar to the KPFM findings acquired on H₂O washed film, our STM topography images did also reveal precipitates on top of the CIGSe surface. Some of these agglomerates are highlighted with a black circle on the surface of the water rinsed sample Figure 5a. The inset depicts the same highlighted region, where a sobel-type filter was applied to enhance contrast (see Supporting Information for full image including a comparison to the H₂O rinsed samples measured with AFM). The precipitations were absent after ammonia treatment (see Figure 5e), consolidating the finding that rinsing the sample only with deionized water was not sufficient to remove all the surface residues.

In Figure 5b–h, the dI/dU -CITS maps of the water rinsed as well as the ones of the ammonia rinsed are depicted. In both cases, we could not identify a distinct contrast in the LDOS contrast at the grain boundaries, similar to the KPFM measurements. However, we did identify variations between different grains and within individual grains, which are attributed to facet related changes in the LDOS. The absence of a pronounced grain boundary contrast is distinct to most of the published CIGSe STM/STS results where a lower density of defect states^[43] ascribed to different degrees of oxidation^[44] of the absorber after exposing them to air or to some additional defect states induced by KCN etching^[45] on grain boundaries were reported. However, all these measurements were carried out on samples that did not undergo a PDT treatment.^[43–47] In our analysis we did not observe a prominent

grain boundary contrast for the NH₄OH cleaned NaF nor RbF treated absorbers.

The LDOS spectra of the different samples are presented in Figure 6. They were derived by computing the median value for each specific voltage of the measured $I(U)$ curve. The median value was preferred here, since there were quite some outliers in the individual $I(U)$ curves, which makes the use of an arithmetic mean curve not meaningful. The presented data shown here can therefore be considered as the average dI/dU curve. Furthermore, we did observe facet dependent contrast, which is a direct consequence of different work functions. These will also change the dI/dU spectra.^[48] The median value of the dI/dU curve again averages out the facet dependence. The curves therefore represent the average dI/dU curve for the most prominent workfunction.

The derivative of the $I(U)$ curve yields the dI/dU , which is directly proportional to the density of states of the sample, the tip and the transmission coefficient.^[49,50] The later one depends exponentially on the applied voltage, which often leads to misinterpretations of the surface bandgap. A normalization with I/V was therefore introduced, which in the case of semiconductors, needs to be broadened to prevent divergences inside the bandgap.^[51] This procedure was applied successfully for other semiconductors in the past and we have adapted the same procedure here.^[48,51,52]

In Figure 6, we compare the LDOS spectra acquired on H₂O and NH₄OH rinsed RbF and NaF-treated samples. Each sample was measured at different spots and repeated with different tips. We observed some scattering, mostly at negative voltages (tunneling from filled substrate states into empty tip states),

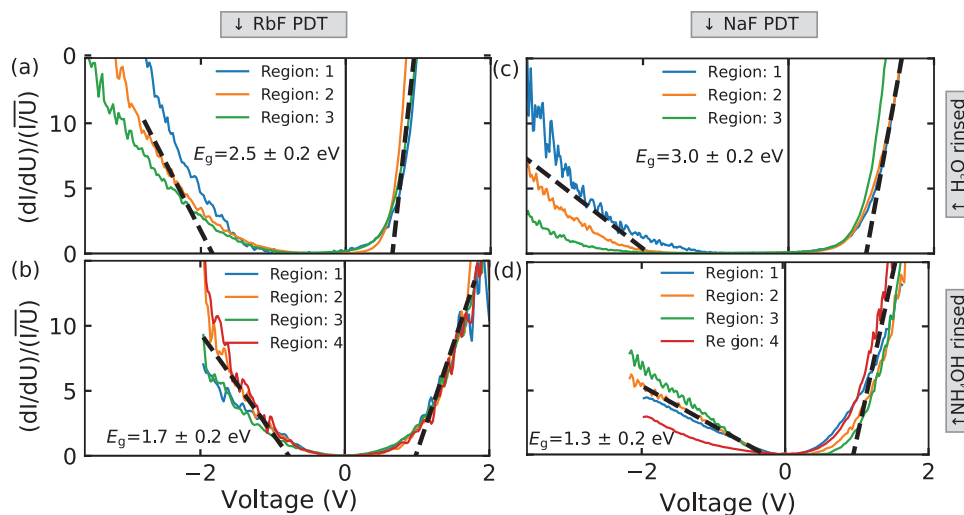


Figure 6. Normalized average dI/dU spectra extracted from a,b) RbF-PDT sample and c,d) NaF-PDT treated sample. (a,c) were cleaned with H_2O whereas (b,d) with NH_4OH . The measurements were carried out on different regions microscopically distinct one to another. Dotted line depicts an average linear extrapolation of the valence and conduction bands for the average of all regions.

which we attribute to different tip density of states. The dotted line is a linear fit to the average of the measured curves. The error of ± 0.2 eV equals to the mean standard deviation of all spectra shown in Figure 6 (≈ 100 meV). In addition, the measurements were done at room temperature which limits the energy resolution of the STM to approximately $3.5 k_B T$, that is, (≈ 100 meV). The error bar is therefore reasonable, given the experimental constraints.

We will first discuss the RbF-treated samples and only then compare them to the NaF-samples. The H_2O cleaned surfaces (Figure 6a) showed a strongly enlarged surface bandgap, compared the bulk CIGSe bandgap (≈ 1.2 eV) in contrast to the NH_4OH rinsed samples (Figure 6b). A value of $E_g = 2.5$ eV was deduced for the H_2O treated sample compared to $E_g = 1.7$ eV for the NH_4OH treated one. The value is larger than the bulk bandgap, in agreement with a Cu-depleted CIGSe surface.^[53] In addition to the reduction of the bandgap, the Fermi-level position is different. The H_2O rinsed sample exhibited a Fermi-level position, which was closer to the conduction band (n-type), which moved close to midgap after NH_4OH treatment.

The enlarged bandgap and the n-type character of the surface after H_2O cleaning would be in agreement with a $RbInSe_2$ phase.^[54] The bandgap of $RbInSe_2$, as deduced from photoluminescence data on thick coevaporated films was reported to be 2.8 eV.^[54] Density function theory calculations of the $RbInSe_2$ phase showed that the native defects with low formation energies were donor-type.^[54] Consequently, the measured surface bandgap and the n-type character of the films are in agreement with a $RbInSe_2$ film. However, the NH_4OH samples did not show signs of this phase anymore. The bandgap is reduced and the n-type character is absent. Therefore, these results suggest that the NH_4OH treated films are not covered with a $RbInSe_2$ phase anymore in agreement with the XPS, KPFM and SIMS results.

The results on the NaF-treated samples are presented in Figure 6c,d. Surprisingly we also measured a strongly enlarged surface bandgap after H_2O cleaning, which cannot be explained with a Rb-rich phase (no Rb-PDT). The bandgap is even slightly

larger than the RbF-case. At first sight this seems to be inconsistent. However, it is well known that the CIGSe surface is extremely sensitive to oxidation. Large surface bandgaps have also been measured via photoelectron spectroscopy techniques, even in the absence of PDTs.^[55] Only after mild sputtering the native oxides could be removed, which revealed the true surface bandgap. The results on the NaF treated samples therefore shed new light on the Rb-treated sample too. Although, the surface bandgap is in agreement with $RbInSe_2$ it is likely that the H_2O cleaned surfaces still suffer from a substantial amount of oxidation (In_2O_3 , Ga_2O_3). The slightly different bandgaps deduced for both sample types indicates that there was indeed a different phase present. However, an unambiguous identification was not possible. The comparison between the NaF and RbF treated samples after H_2O rinsing allows us to conclude that the high surface bandgaps are not necessarily due to a $RbInSe_2$ layer. The H_2O rinse, combined with Na and Rb on top most probably leads to a slight oxidation, which in turn leads to large surface bandgap. The existence of such oxides have already been reported for Rb-treated CIGSe absorbers.^[16] Due to the large scattering of the dI/dU spectra a negative voltages, we are not able to disentangle small amounts of oxides from a $RbInSe_2$. A dedicated analysis of the different oxides present at the surface has not been carried out in this study. We note however that the oxygen/indium ratio on NH_4OH cleaned surfaces are approximately a factor of two lower compared to the H_2O cleaned surfaces.

Fortunately, the situation changes again after the NH_4OH rinsing. The surface bandgaps reduce and we do estimate a slightly higher value for the Rb-treated sample compared to the NaF-treated one (1.7 vs. 1.3 eV). The surface bandgaps of the films were not compatible with the bulk CIGSe. The values are enlarged, which is a well-known property of Cu(In,Ga)Se₂. The Cu-depletion at the surface has often been attributed to the formation of ordered vacancy compounds^[53,56] or completely Cu depleted surfaces.^[57–59] The Cu-deficient layers, such as $CuIn_3Se_5$, $CuIn_5Se_8$, or Cu-deficient surface reconstructions

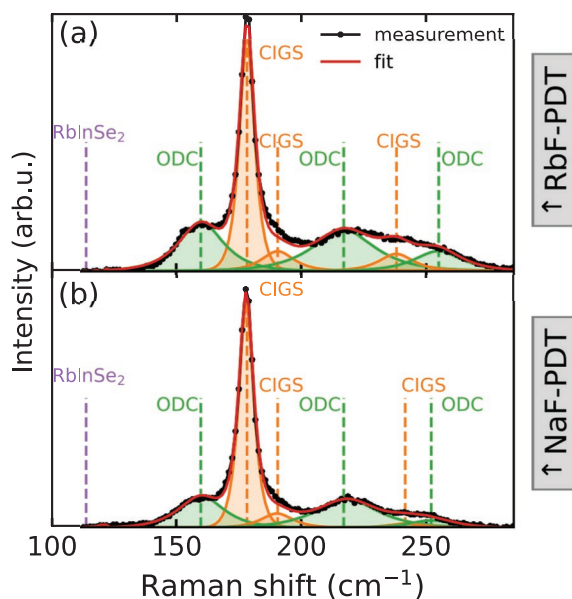


Figure 7. Raman spectra of the a) RbF PDT and NH_4OH rinsed sample, b) NaF PDT and NH_4OH rinsed sample. Each peak was fitted with six peaks representing the CIGSe A_1 and the B_2/E modes and their respective peaks due ordered defect compounds labeled ODC, representing the copper depleted phases.

exhibit different electronic properties, with slightly enlarged bandgaps^[60,61] compared to the chalcopyrite phase. The STM data suggests that especially after NH_4OH rinsing the surface is composed of such a very thin layer with a slightly enlarged bandgap. However, it needs to be taken into account that there is still some Rb left at the surface, as corroborated by XPS and SIMS, which makes the Cu-deficient layer distinct from the non-PDT treated Cu-poor surface compositions. The STS data supports this conclusion since we measure slightly enlarged bandgaps for the Rb-treated sample compared to the Na-one. The results are in agreement with the KPFM measurements, where an increase of the work function was observed after NH_4OH cleaning, corroborating a change in the surface composition between H_2O and NH_4OH .

In order to further corroborate the absence of RbInSe_2 on the RbF-PDT treated sample after NH_4OH rinsing and confirm the existence of a Cu-depleted phase, Raman spectroscopy was employed. In Figure 7, a NH_4OH rinsed Rb-PDT treated sample was compared with a NH_4OH NaF-PDT treated sample. Based on available literature^[62,63] we attribute three peaks in Figure 7a,b to CIGSe, namely the A_1 (high intensity mode) and two B_2/E modes. Furthermore three modes were assigned to the copper depleted regions. M. Guc et al.^[64] report for RbInSe_2 three main Raman peaks at 114.3, 179.7, and 238 cm^{-1} . In the Raman spectrum measured on the RbF PDT sample (see Figure 7b), no peak at or around 114.7 cm^{-1} has been observed. Concerning the positions 179 and 238 cm^{-1} we observed peaks in our Raman spectra. However, as stated before, we attribute those peaks to the CIGSe A_1 and the ODC modes and not to Raman modes of RbInSe_2 secondary phases. This argument is supported by comparing the Raman spectrum of the RbF-PDT sample (see Figure 7a) with the spectrum of the NaF-PDT sample (see Figure 7b).

Since we observed the same peaks in the NaF PDT sample where we obviously do not expect any RbInSe_2 secondary phases, we can exclude the possibility of Raman peaks related to RbInSe_2 secondary phases for the positions 179 and 238 cm^{-1} in the Raman spectrum in Figure 7a. Therefore, we conclude that no RbInSe_2 was left after NH_4OH rinsing in agreement with XPS, KPFM, SIMS, and STS.

We also checked if there was a RbInSe_2 secondary phase present after H_2O cleaning. Raman measurements comparing NaF and RbF treated samples with H_2O and NH_4OH cleaning are shown in Supporting Information. We did not observe significant differences between the spectra, indicating that either the RbInSe_2 phase was not present or below the detection limit of the Raman measurements. Considering the CIGSe composition ($\text{Cu}/(\text{In}+\text{Ga}) \approx 0.95$) used in this study and referring to literature, we conclude that the Raman measurements did not allow us to unambiguously proof or disproof the existence of a tiny amount of RbInSe_2 on the surface of our films.

3. Discussion

The preceding multi-modal nanoscale analysis has revealed that the surface of CIGSe absorbers, with a $\text{Cu}/(\text{In}+\text{Ga})$ ratio ≈ 0.95 , cleaned with NH_4OH did not exhibit a measurable RbInSe_2 phase. This result was verified via different surface sensitive measurements. The atomic concentrations as deduced from XPS were not compatible with a RbInSe_2 . We could not identify a significant asymmetry or broadening in the XPS core levels that would hint toward a RbInSe_2 . The SIMS measurements also did not show a significant positive correlation of In and Rb at the surface as we would have expected in the case of a RbInSe_2 . The STS measurements revealed a surface bandgap that only increased slightly, compared to a Cu-depleted NaF surface. In Raman spectroscopy, we did not observe vibrational modes that can be linked to a RbInSe_2 phase.

Despite the absence of a RbInSe_2 phase, we could show that the near surface region was modified after RbF PDT. The Cu-depletion further increased at the surface and was supplemented by almost the same amount of Rb. Consequently, our analysis points toward an exchange of Cu with Rb in the ODC surface layer, which is accompanied by a slight increase in the surface bandgap.

However, care needs to be taken when comparing our results to other literature reports. As already stated before, the existence of a RbInSe_2 layer depends on the Cu-content and exact processing of the CIGSe absorber layer.^[11,16,17] In this case, the samples were intentionally grown close to the stoichiometric point (see Experimental Section). Furthermore, the detection limit of each technique (XPS/Raman) needs to be taken into account when discussing this phase and we have given conclusive evidence that the cleaning procedure needs to be taken into account too. This study however shows that for close to stoichiometric films, exhibiting power conversion efficiencies above 20%, a RbInSe_2 phase is not present. This result is also in accordance with^[16,54] who showed that a RbInSe_2 layer often induces a low fill factor and consequently lower power conversion efficiencies. A partial coverage as suggested in literature^[13] may mitigate these adverse effects. However, in the present case

we have also not determined such a modified surface, although we have used extremely surface sensitive and high resolution techniques. Since we have observed strong improvements in power conversion efficiency due to the Rb-PDT, as reported by many others we conclude that nor a fully covering RbInSe_2 nor a partial coverage of that phase are responsible for the improvements in the solar cell devices.

The question that immediately arises is if this modified near surface region is in fact responsible for the improved device performance. From our analysis we cannot answer this question directly but we can at least rule out some possibilities. The formation of a RbInSe_2 layer can be excluded. Furthermore, we have not observed a systematic change of the grain boundary properties. Our AFM and STM data, which can only measure grain boundary properties at the surface, did not show significant band bending or increased density of states. Furthermore, we have not observed an Rb enrichment at the grain boundaries after NH_4OH cleaning despite the excellent sensitivity of SIMS for Rb (a few ppm). We note that this is due to the surface cleaning itself. Recently, it was shown on absorbers produced at a different institution that Rb decorates the grain boundaries in the bulk whereas no distinct contrast was present at the surface.^[15] Consequently, we can rule out a grain boundary modification in the near surface region, but cannot comment on grain boundaries far away from the surface. It is known from simulations that the interface recombination velocity at the CIGSe/CdS heterojunction is of utmost importance to achieve high efficiencies. We know that both the NaF and RbF PDT treated absorbers exhibit a Cu-depleted surface. The RbF treated absorbers have a Rb enriched ODC as discussed extensively before. In the Supporting Information, we show that a reduction of the interface recombination velocity at the CIGSe/ODC interface could be responsible for the boost in efficiency. This interface is very critical and a Rb-rich ODC may very well have better optoelectronic properties, as compared to the NaF PDT absorbers. Furthermore the number of defects at this interface may simply be lower, which would translate to a lower recombination velocity and thereby a higher performance. Here additional theoretical calculations would be needed to better understand how Rb substituted ODCs compare to a Cu-based ODCs.

Although we could use the argument of a reduced interface recombination velocity to explain our data, we are also aware that a similar boost in efficiency can also be achieved with a reduced bulk defect density or increased doping. In that sense, our surface sensitive measurements do not allow to filter out only one possible solution.

One very important aspect, that became clear throughout this manuscript is that the use of RbF/NaF leads, in all cases to precipitates that need to be removed. The proper choice of the chemical solution is very important and it will modify the surface again. The problem is very important for dry buffers and dry inline processing where a NH_4OH treatment is simply not an option or very cumbersome. A possible way out could be the use of alkali metal dispensers, as previously shown for the case of K and Rb.^[65,66] The use of pure alkali metals evaporated at elevated temperatures on to a CIGSe surface should modify the near surface region (exchange of Cu with Rb) without the formation of secondary phases, however the amount needs to be tuned to avoid the formation of other unwanted secondary phases.

4. Conclusion

Our multimodal nanoscale analysis of PDT treated CIGSe absorbers has revealed that the surface composition depends sensitively on the cleaning procedure. We have identified Rb-rich patches at the surface of H_2O rinsed absorbers, which were removed after NH_4OH cleaning. From XPS these patches could be assigned to a RbInSe_2 phase. However, the SIMS data did not show a strong correlation between In and Rb at the surface. Furthermore, the surface bandgaps after H_2O cleaning, as measured via STS are very similar for the RbF and NaF samples.

After NH_4OH cleaning, the surface bandgaps, the composition, the elemental distributions on the nanoscale and the vibrational modes do not support the model of the RbInSe_2 phase present at the surface of these high efficiency CIGSe absorbers. The compositional ratios deduced from XPS suggest that Rb substitutes Cu in the ODC layer, which is intrinsically present on Cu-poor surfaces. This substitution leads to a slight increase in surface bandgap as shown via STS measurements. This Rb-rich ODC layer is one critical parameter that needs to be taken into account when discussing the improvements in power conversion efficiency after RbF treatment. Although the results presented here are limited to the first 10 nm of the absorbers, they give important guidelines for future theoretical and experimental work. From a device point of view the occurrence of secondary phases after growth needs to be circumvented in order to allow for an all vacuum/dry processing of devices and modules. Furthermore, more fundamental theoretical work on the interaction of heavy alkali elements with ODCs and the CIGSe bulk is needed.

5. Experimental Section

The $\text{Cu(In,Ga)}\text{Se}_2$ samples used in this study were prepared at EMPA via multistage coevaporation on Mo coated soda lime glass substrates, including a 180 nm SiO_2 Na diffusion barrier. A schematic representation of the growth processes, including the substrate temperature and the deposition times for each stage are depicted in Figure 8. The two sample types analyzed in this study are denoted as RbF-PDT and NaF-PDT in Figure 8. The bulk composition as measured via X-Ray fluorescence were 0.95 (NaF-PDT) and 0.96 (RbF-PDT) for the $\text{Cu}/(\text{In}+\text{Ga})$ ratios and

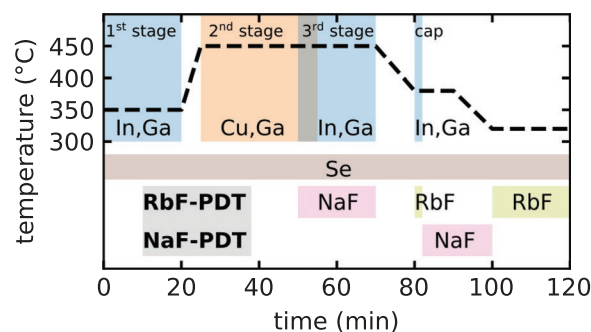


Figure 8. Sketch of the CIGSe deposition process. The dashed line depicts the substrate temperature during deposition. The colored boxes indicate which elements are deposited at which time. Two sets of samples were investigated, denoted as RbF-PDT and NaF-PDT. More details on the experimental process can be found in ref. [67].

0.43 for the Ga/(In+Ga). Within the errorbar of the measurement, both samples exhibited the same bulk composition.

A more detailed description of the processes, including device results were reported in ref. [67]. The RbF-PDT samples reach power conversion efficiencies up to 20.8 %, whereas the NaF-PDT samples only reach efficiencies in the range of 18 %. The CIGSe samples were received in a nitrogen sealed box without air exposure. The transport took less than 12 h in total and the samples were subsequently stored in a N₂-filled glove box with oxygen and H₂O levels of approximately 1 ppm.

The samples were measured as-grown, after H₂O rinsing and after NH₄OH rinsing. The H₂O rinsing was done as follows: The samples were removed from the N₂-filled glovebox and immediately immersed in distilled water for 60 s. Subsequently, they were taken out of beaker and blown dry with an inclined flow of nitrogen while transferring them back to the glovebox. For the NH₄OH rinsing two clean beakers were used, one with 1M solution of ammonium hydroxide (NH₄OH) and the other with distilled water. The samples were first immersed in NH₄OH for 180 s and then immersed in distilled water for 60 s followed by an immediate transfer to the glovebox. All samples were mounted in the glovebox and transferred to the UHV STM/XPS system or the N₂-filled AFM system via dedicated transfer systems without additional exposure to ambient conditions. For the XPS and STM measurements, the procedure described above was carried out in a N₂ filled glove-bag connected to antechamber of the glovebox, to further reduce the oxygen contamination. The glove-bag was omitted for the KPFM and AFM measurements carried out in a N₂ atmosphere since there a residual oxygen and moisture level of ≈5% was present during the measurements.

XPS measurements were carried out in ultra high vacuum with a non-monochromatic Al K_α source. For all samples, a survey spectrum and dedicated high resolution spectra for the elements of interest were recorded. The peak shape, which is determined by the detector settings was deduced from measurements carried out on epitaxial CIGSe samples similar to the ones reported in ref. [65]. The intensity of each core level were corrected via the elemental relative sensitivity factors given by ref. [40] and the detector corrections supplied by the company (Prevac) were used. No other corrections have been made. According to ref. [68] this is a valid approximation to about 15%.

Kelvin Probe Force Microscopy measurements were carried out in a N₂ filled glovebox with oxygen and water levels below 5 %. The topography was measured in amplitude modulation (AM) mode, whereas the KPFM signal was acquired in frequency modulation (FM) mode. Calibration of the tip work function was carried out on freshly cleaved highly oriented pyrolytic graphite with a workfunction of 4.6 eV ± 0.1 eV.^[69]

The scanning tunneling microscopy and spectroscopy measurements were carried out in the same variable temperature ultra-high vacuum system as the XPS. Tungsten tips were chemically etched and cleaned in situ on clean Au substrates. Local density of states (LDOS) maps were acquired via current imaging tunneling spectroscopy (CITS) maps at different regions of the samples with the aim to get representative data. The measured areas vary from 600 × 600 nm² to 2 × 2 μm². For each CITS map, a grid of 150 × 150 pixels was defined and local current-voltage spectra were recorded, while the feedback loop was switched off. Subsequently, the LDOS, which is proportional to dI/dU ^[70] was extracted by numerical differentiation of the current I with respect to the applied voltage U .

A Helium Ion Microscope equipped with a double focusing magnetic sector secondary ion mass spectrometer (HIM-SIMS) was used to correlate secondary electron imaging at nanometer resolution with chemical composition mapping at 15 nm resolution.^[30] All samples were transported in N₂ filled containers to the HIM-SIMS apparatus to limit oxidation. In the present study, the HIM-SIMS was operated with a 20 keV Ne⁺ primary ion beam to sputter away approximately 10 nm of the surface. A certain fraction of the ejected atoms are spontaneously ionized during the sputtering process. These secondary ions were collected by the SIMS spectrometer where they were filtered according to their mass-to-charge ratio (m/z), and detected. The SIMS was operated

in imaging mode to map the following elements: In positive mode, that is, collecting positive ions: Na, Ga, Rb, In. The elements measured in negative mode were O, F, and Se. Due to the characteristics of the operating mode, the positive and negative ions cannot be detected simultaneously. Therefore, it was not possible to collect maps of all the elements on the same spot from the same depth. In the present case, the measurements were done sequentially on different spots. The maps discussed throughout this manuscript are average intensities from the first 10 nm of the film. Due to matrix effects, which affects the ionisation yield, the intensity cannot be converted to a concentration. However, the mapping allows to resolve chemical heterogeneities with high spatial resolution and high sensitivity.

Raman spectra were acquired to identify possible secondary phases (ordered vacancy compound, AlInSe₂) on top of the CIGSe absorbers. The measurements were carried out in micro Raman setup under ambient conditions with a 532 nm laser, 2400 $\frac{1}{\text{mm}}$ grating and a power of 452 μW and a spot size of approximately 1 μm, which was sufficiently low to prevent damage of the sample.

Supporting Information

Supporting Information is available from the Wiley Online Library or from the author.

Acknowledgements

This research was funded in whole, or in part, by the Luxembourg National Research Fund (FNR), grant reference [11244141,11696002, 12246511,13584473]. For the purpose of open access, the author has applied a Creative Commons Attribution 4.0 International (CC BY 4.0) license to any Author Accepted Manuscript version arising from this submission. The authors acknowledge useful discussions with Evandro Lanzoni and Jeremy Hieulle. Technical support from Bernd Uder, Ulrich Siegel, Michele Melchiorre and Thomas Schuler was acknowledged.

Conflict of Interest

The authors declare no conflict of interest.

Data Availability Statement

The data that support the findings of this study are available from the corresponding author upon reasonable request.

Keywords

CIGSe, PDT treatment, thin film solar cells

Received: January 16, 2023

Revised: March 21, 2023

Published online: May 7, 2023

[1] M. Nakamura, K. Yamaguchi, Y. Kimoto, Y. Yasaki, T. Kato, H. Sugimoto, *IEEE J. Photovoltaics* **2019**, 9, 1863.

[2] M. Green, E. Dunlop, J. Hohl-Ebinger, M. Yoshita, N. Kopidakis, X. Hao, *Prog. Photovoltaics Res. Appl.* **2022**, 30, 3.

- [3] A. Chirila, P. Reinhard, F. Pianezzi, P. Bloesch, A. R. Uhl, C. Fella, L. Kranz, D. Keller, C. Gretener, H. Hagendorfer, D. Jaeger, R. Erni, S. Nishiwaki, S. Buecheler, A. N. Tiwari, *Nat. Mater.* **2013**, 12, 1107.
- [4] P. Reinhard, F. Pianezzi, B. Bissig, A. Chirila, P. Blösch, S. Nishiwaki, S. Buecheler, A. N. Tiwari, *IEEE J. Photovoltaics* **2015**, 5, 656.
- [5] P. Jackson, R. Wuerz, D. Hariskos, E. Lotter, W. Witte, M. Powalla, *Phys. Status Solidi RRL* **2016**, 10, 583.
- [6] E. Handick, P. Reinhard, J. H. Alsmeyer, L. Köhler, F. Pianezzi, S. Krause, M. Gorgoi, E. Ikenaga, N. Koch, R. G. Wilks, S. Buecheler, A. N. Tiwari, M. Bär, *ACS Appl. Mater. Interfaces* **2015**, 7, 27414.
- [7] D. Hauschild, D. Kreikemeyer-Lorenzo, P. Jackson, T. M. Friedlmeier, D. Hariskos, F. Reinert, M. Powalla, C. Heske, L. Weinhardt, *ACS Energy Lett.* **2017**, 2, 2383.
- [8] B. Ürsür, N. Maticiu, T. Kodalle, R. Wenisch, I. Majumdar, Y. Wang, H. A. Yetkin, T. Bertram, C. A. Kaufmann, R. Schlattmann, I. Lauermaun, *Renewable Energy* **2021**, 180, 626.
- [9] N. Nicoara, R. Manaligod, P. Jackson, D. Hariskos, W. Witte, G. Sozzi, R. Menozzi, S. Sadewasser, *Nat. Commun.* **2019**, 10, 1.
- [10] M. Malitckaya, H. P. Komsa, V. Havu, M. J. Puska, *J. Phys. Chem. C* **2017**, 121, 15516.
- [11] N. Taguchi, S. Tanaka, S. Ishizuka, *Appl. Phys. Lett.* **2018**, 113, 11.
- [12] E. Handick, P. Reinhard, R. G. Wilks, F. Pianezzi, T. Kunze, D. Kreikemeyer-Lorenzo, L. Weinhardt, M. Blum, W. Yang, M. Gorgoi, E. Ikenaga, D. Gerlach, S. Ueda, Y. Yamashita, T. Chikyow, C. Heske, S. Buecheler, A. N. Tiwari, M. Bär, *ACS Appl. Mater. Interfaces* **2017**, 9, 3581.
- [13] J. Bombsch, E. Avancini, R. Carron, E. Handick, R. Garcia-Diez, C. Hartmann, R. Félix, S. Ueda, R. G. Wilks, M. Bär, *ACS Appl. Mater. Interfaces* **2020**, 12, 34941.
- [14] E. Ghorbani, J. Kiss, H. Mirhosseini, G. Roma, M. Schmidt, J. Windeln, T. D. Kühne, C. Felser, *J. Phys. Chem. C* **2015**, 119, 25197.
- [15] A. Elizabeth, S. K. Sahoo, H. Phirke, T. Kodalle, D. Kühne, A. Redinger, C. A. Kaufmann, H. Mirhosseini, *ACS Appl. Mater. Interfaces* **2022**, 14, 34101.
- [16] N. Maticiu, T. Kodalle, B. Ürsür, T. Bertram, R. Wenisch, Y. Wang, I. Majumdar, H. A. Yetkin, D. Abou-Ras, N. Schäfer, C. A. Kaufmann, R. Schlattmann, I. Lauermaun, *Sol. Energy Mater. Sol. Cells* **2021**, 226, 111071.
- [17] S. Siebentritt, E. Avancini, M. Bär, J. Bombsch, E. Bourgeois, S. Buecheler, R. Carron, C. Castro, S. Duguay, R. Félix, E. Handick, D. Hariskos, V. Havu, P. Jackson, H. P. Komsa, T. Kunze, M. Malitckaya, R. Menozzi, M. Nesladek, N. Nicoara, M. Puska, M. Raghuvanshi, P. Pareige, S. Sadewasser, G. Sozzi, A. N. Tiwari, S. Ueda, A. Vilalta-Clemente, T. P. Weiss, F. Werner, et al., *Adv. Energy Mater.* **2020**, 10, 8.
- [18] Y. F. Zheng, L. Huang, B. Li, R. Wang, S. H. Wei, *Phys. Rev. Appl.* **2021**, 15, 1.
- [19] P. Schöppe, S. Schönherr, R. Wuerz, W. Wisniewski, G. Martínez-Criado, M. Ritzer, K. Ritter, C. Ronning, C. S. Schnohr, *Nano Energy* **2017**, 42, 307.
- [20] T. Wirtz, O. De Castro, J. N. Audinot, P. Philipp, *Annu. Rev. Anal. Chem.* **2019**, 12, 523.
- [21] O. Cojocaru-Mirédin, M. Raghuvanshi, R. Wuerz, S. Sadewasser, *Adv. Funct. Mater.* **2021**, 31, 2103119.
- [22] D. Abou-Ras, A. Nikolaeva, S. Caicedo Dávila, M. Krause, H. Guthrey, M. Al-Jassim, M. Morawski, R. Scheer, *Solar RRL* **2019**, 3, 8.
- [23] M. H. Wolter, R. Carron, E. Avancini, B. Bissig, T. P. Weiss, S. Nishiwaki, T. Feurer, S. Buecheler, P. Jackson, W. Witte, S. Siebentritt, *Prog. Photovolt Res Appl.* **2022**, 30, 702.
- [24] E. M. Lanzoni, T. Gallet, C. Spindler, O. Ramírez, C. K. Boumenou, S. Siebentritt, A. Redinger, *Nano Energy* **2021**, 88, 106270.
- [25] M. H. Wolter, B. Bissig, E. Avancini, R. Carron, S. Buecheler, P. Jackson, S. Siebentritt, *IEEE J. Photovoltaics* **2018**, 8, 1320.
- [26] H. Lee, Y. Jang, S. W. Nam, C. Jung, P. P. Choi, J. Gwak, J. H. Yun, K. Kim, B. Shin, *ACS Appl. Mater. Interfaces* **2019**, 11, 35653.
- [27] F. Pianezzi, P. Reinhard, A. Chirila, B. Bissig, S. Nishiwaki, S. Buecheler, A. N. Tiwari, *PCCP* **2014**, 16, 8843.
- [28] R. Wuerz, W. Hempel, P. Jackson, *J. Appl. Phys.* **2018**, 124, 16.
- [29] T. Kodalle, M. D. Heinemann, D. Greiner, H. A. Yetkin, M. Klupsch, C. Li, P. A. van Aken, I. Lauermaun, R. Schlattmann, C. A. Kaufmann, *Solar RRL* **2018**, 2, 1.
- [30] J. N. Audinot, P. Philipp, O. De Castro, A. Biesemeier, Q. H. Hoang, T. Wirtz, *Rep. Prog. Phys.* **2021**, 84, 105901.
- [31] M. Burgelman, P. Nollet, S. Degraeve, *Thin Solid Films* **2000**, 361, 527.
- [32] N. Maticiu, T. Kodalle, J. Lauche, R. Wenisch, T. Bertram, C. A. Kaufmann, I. Lauermaun, *Thin Solid Films* **2018**, 665, 143.
- [33] E. Avancini, R. Carron, T. P. Weiss, C. Andres, M. Bürki, C. Schreiner, R. Figi, Y. E. Romanyuk, S. Buecheler, A. N. Tiwari, *Chem. Mater.* **2017**, 29, 9695.
- [34] T. Kodalle, M. D. Heinemann, D. Greiner, H. A. Yetkin, M. Klupsch, C. Li, P. A. van Aken, I. Lauermaun, R. Schlattmann, C. A. Kaufmann, *Solar RRL* **2018**, 2, 9.
- [35] R. Hertwig, S. Nishiwaki, M. Ochoa, S. C. Yang, T. Feurer, E. Gilshtein, A. N. Tiwari, R. Carron, *EPJ Photovoltaics* **2020**, 11, 2020.
- [36] F. Larsson, O. Donzel-Gargand, J. Keller, M. Edoff, T. Törndahl, *Sol. Energy Mater. Sol. Cells* **2018**, 183, 8.
- [37] W. Witte, W. Hempel, S. Paetel, R. Menner, D. Hariskos, *ECS J. Solid State Sci. Technol.* **2021**, 10, 055006.
- [38] S. W. Gaarenstroom, N. Winograd, *J. Chem. Phys.* **1977**, 67, 3500.
- [39] B. Canava, J. Vigneron, A. Etcheberry, J. F. Guillemoles, D. Lincot, *Appl. Surf. Sci.* **2002**, 202, 8.
- [40] J. H. Scofield, *J. Electron. Spectrosc. Relat. Phenom.* **1976**, 8, 129.
- [41] S. Ishizuka, N. Taguchi, J. Nishinaga, Y. Kamikawa, S. Tanaka, H. Shibata, *J. Phys. Chem. C* **2018**, 122, 3809.
- [42] K. Pearson, *Proc. R. Soc. London* **1895**, 58, 240.
- [43] H. Mönig, Y. Smith, R. Caballero, C. A. Kaufmann, I. Lauermaun, C. M. Lux-Steiner, S. Sadewasser, *Phys. Rev. Lett.* **2010**, 105, 11.
- [44] A. Elizabeth, S. K. Sahoo, D. Lockhorn, A. Timmer, N. Aghdassi, H. Zacharias, T. D. Kühne, S. Siebentritt, H. Mirhosseini, H. Mönig, *Phys. Rev. Mater.* **2020**, 4, 6.
- [45] C. K. Boumenou, F. Babbe, A. Elizabeth, M. Melchiorre, C. Spindler, J. Guillot, H. Mönig, S. Siebentritt, A. Redinger, *Phys. Rev. Mater.* **2020**, 4, 4.
- [46] S. Bröcker, D. Kück, A. Timmer, I. Lauermaun, B. Ürsür, D. Greiner, C. A. Kaufmann, H. Mönig, *ACS Appl. Mater. Interfaces* **2015**, 7, 13062.
- [47] H. Mönig, D. Lockhorn, N. Aghdassi, A. Timmer, C. A. Kaufmann, R. Caballero, H. Zacharias, H. Fuchs, *Adv. Mater. Interfaces* **2014**, 1, 2.
- [48] T. Gallet, D. Grabowski, T. Kirchartz, A. Redinger, *Nanoscale* **2019**, 11, 16828.
- [49] C. J. Chen, *Introduction to scanning tunneling microscopy: Monographs on the physics and chemistry of materials*, vol. 69, 3rd Ed., **2021**.
- [50] C. Wagner, R. Franke, T. Fritz, *Phys. Rev. B: Condens. Matter Mater. Phys.* **2007**, 75, 1.
- [51] R. M. Feenstra, *Phys Rev B* **1994**, 50, 4561.
- [52] F. W. Herbert, A. Krishnamoorthy, K. J. V. Vliet, B. Yildiz, *Surf. Sci.* **2013**, 618, 53.
- [53] D. Schmid, M. Ruckh, F. Grunwald, H. W. Schock, *J. Appl. Phys.* **1993**, 73, 2902.
- [54] T. Kodalle, T. Bertram, R. Schlattmann, C. A. Kaufmann, *IEEE J. Photovoltaics* **2019**, 9, 18.
- [55] M. Bär, S. Nishiwaki, L. Weinhardt, S. Pookpanratana, O. Fuchs, M. Blum, W. Yang, J. D. Denlinger, W. N. Shafarman, C. Heske, *Appl. Phys. Lett.* **2008**, 93, 24.
- [56] S. B. Zhang, S. H. Wei, A. Zunger, *Phys. Rev. Lett.* **1997**, 78, 4059.
- [57] H. Mönig, C. H. Fischer, R. Caballero, C. A. Kaufmann, N. Allsop, M. Gorgoi, R. Klenk, H. W. Schock, S. Lehmann, M. C. Lux-Steiner, I. Lauermaun, *Acta. Mater.* **2009**, 57, 3645.

- [58] J. E. Jaffe, A. Zunger, *Phys. Rev. B: Condens. Matter Mater. Phys.* **2001**, 64, 2413041.
- [59] D. Liao, A. Rockett, *J. Appl. Phys.* **2002**, 91, 1978.
- [60] T. Maeda, W. Gong, T. Wada, *Jpn. J. Appl. Phys.* **2016**, 55, 04ES15.
- [61] A. Sharan, F. P. Sabino, A. Janotti, N. Gaillard, T. Ogitsu, J. B. Varley, *J. Appl. Phys.* **2020**, 127, 6.
- [62] C. Rincón, S. M. Wasim, G. Marín, J. M. Delgado, J. R. Huntzinger, A. Zwick, J. Galibert, *Appl. Phys. Lett.* **1998**, 73, 441.
- [63] T. Kodalle, L. Choubrac, L. Arzel, R. Schlatmann, N. Barreau, C. A. Kaufmann, *Sol. Energy Mater. Sol. Cells* **2019**, 200, 109997.
- [64] M. Guc, T. Kodalle, R. Kormath Madam Raghupathy, H. Mirhosseini, T. D. Kühne, I. Becerril-Romero, A. Pérez-Rodríguez, C. A. Kaufmann, V. Izquierdo-Roca, *J. Phys. Chem. C* **2020**, 124, 1285.
- [65] E. M. Lanzoni, O. Ramírez, H. Phirke, A. Elizabeth, H. Mönig, A. Redinger, *Thin Solid Films* **2022**, 741, 139002.
- [66] M. Edoff, T. Torndahl, F. Larsson, O. Stolt, N. Shariati-Nilsson, L. Stolt, *Conference Record of the IEEE Photovoltaic Specialists Conference*, IEEE, Chicago, IL, USA **2019**, pp. 618–621.
- [67] R. Carron, S. Nishiwaki, T. Feurer, R. Hertwig, E. Avancini, J. Löckinger, S.-C. Yang, S. Buecheler, A. N. Tiwari, *Adv. Energy Mater.* **2019**, 9, 1900408.
- [68] S. Hofmann, *Auger- and X-Ray Photoelectron Spectroscopy in Materials Science : A User-Oriented Guide*, vol. 49, Springer, Berlin **2013**.
- [69] M. M. Beerbom, B. Lägél, A. J. Cascio, B. V. Doran, R. Schlaf, *J. Electron. Spectrosc. Relat. Phenom.* **2006**, 152, 12.
- [70] C. J. Chen, *Introduction to Scanning Tunneling Microscopy*, Oxford University Press, Oxford **2007**.